



Cite this: *Chem. Sci.*, 2025, **16**, 19702

All publication charges for this article have been paid for by the Royal Society of Chemistry

Received 26th June 2025  
Accepted 19th September 2025

DOI: 10.1039/d5sc04731e  
[rsc.li/chemical-science](http://rsc.li/chemical-science)

## Introduction

Carbon capture is an attractive strategy for mitigating anthropogenic CO<sub>2</sub> emissions to curb global climate change. Developing this technology is especially important for sectors where emissions are hard to abate through other means, such as the cement or steel industry. Currently, most deployed carbon capture systems rely on liquid sorbents that must be thermally regenerated when saturated.<sup>1</sup> This energy-consuming step substantially raises operational costs, thus presenting a barrier to the widespread adoption of the technology. In addition, the regeneration step has a large CO<sub>2</sub> footprint, thus partially offsetting the benefits of the capture process.<sup>2</sup> As such, developing more sustainable approaches to carbon capture is a timely challenge.

Recently, carbon capture methods relying on electrochemical regeneration have garnered significant attention as sustainable, efficient, and safe alternatives to the traditional thermal approach.<sup>1-3</sup> In many of these methods, low-cost electricity is used to reversibly interconvert a molecular redox mediator between two redox states, where one state leads to CO<sub>2</sub> capture while the other leads to CO<sub>2</sub> release.

In the simplest redox-mediated electrochemical approach, direct binding, an initially unreactive mediator is reduced to a more nucleophilic state where it can temporarily bind electrophilic CO<sub>2</sub>.<sup>4</sup> Upon reoxidation of the mediator, its nucleophilicity is lowered and CO<sub>2</sub> is released. This strategy has been demonstrated in non-aqueous media with disulfides,<sup>5</sup> pyridines,<sup>6</sup> and quinones.<sup>7</sup> However, in this method, the use of organic solvent as the electrolyte is undesirable from a cost and safety standpoint. A more elaborate approach, pH-swing, involves the reversible switching of the mediator's basicity through proton-coupled electron transfer (PCET).<sup>8</sup> The principle of pH-swing CO<sub>2</sub> capture/release is illustrated in Fig. 1A. The reduction of the redox mediator consumes protons in the electrolyte, causing an increase in the electrolyte pH and the capture of CO<sub>2</sub> as carbonate or bicarbonate. Upon reoxidation, the mediator releases protons, leading to a decrease in the electrolyte pH and the release of CO<sub>2</sub>. A key advantage of the pH-swing strategy is that the capture/release process occurs in water, which reduces operational costs, increases the system's safety, and enables high current densities. Several pH-swing mediator motifs have been reported, such as quinones,<sup>9,10</sup> phenazines,<sup>11-15</sup> 1-aminopyridinium,<sup>16</sup> riboflavin,<sup>17</sup> and guanidines.<sup>18</sup> However, the field is still nascent, and the exploration of further molecules is critical to enlarging the library of viable mediators.

Herein, we report pH-swing carbon capture based on 4-substituted acylpyridinium mediators. These molecules are synthesized in 1-2 steps and are isolated through a simple filtration, which is ideal for scale-up. The acylpyridinium molecular family was previously investigated for aqueous redox flow batteries by Sevov *et al.* and found to induce pH changes

<sup>a</sup>Department of Chemistry, University of Toronto, Lash Miller Chemical Laboratories, 80 St. George Street, Toronto, Ontario, M5S 3H6, Canada

<sup>b</sup>Department of Chemical Engineering and Applied Chemistry, University of Toronto, 200 College Street, Toronto, Ontario, M5S 3E5, Canada. E-mail: [dwight.seferos@utoronto.ca](mailto:dwight.seferos@utoronto.ca)

<sup>c</sup>Clean Energy Innovation Research Centre (CEI), National Research Council Canada, 2620 Speakman Drive, Mississauga, Ontario, L5K 2L1, Canada. E-mail: [shuai.chen@nrc-cnrc.gc.ca](mailto:shuai.chen@nrc-cnrc.gc.ca)

† These two authors contributed equally.



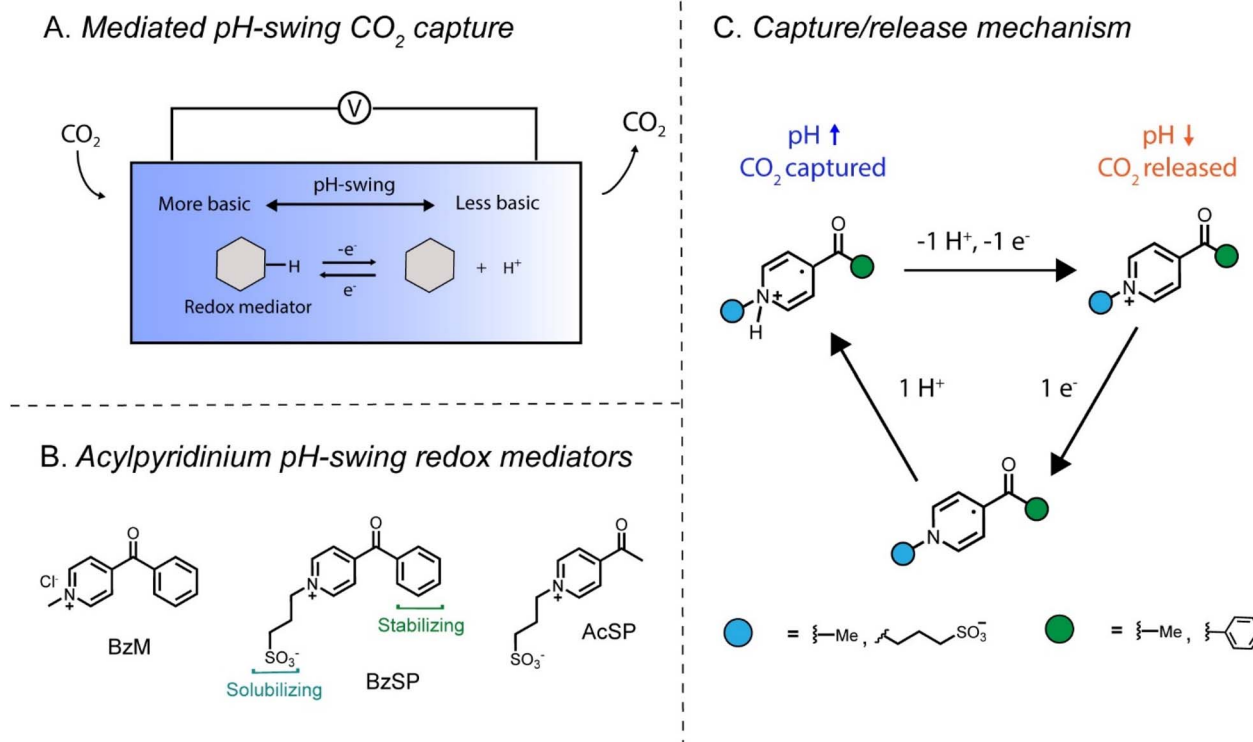


Fig. 1 (A) General scheme for redox-mediated pH-swing carbon capture in one compartment. (B) Acylpyridinium redox mediators used in this work. (C) Mechanism of  $\text{CO}_2$  capture with pyridinium mediators.

due to proton abstraction.<sup>19</sup> In this work, we exploit this property to mediate cyclical  $\text{CO}_2$  capture.

The pyridinium mediators are synthesized in their oxidized form and can be reduced through PCET to form stable radicals. The solubility and radical stability of the mediators can be influenced by the group at the *N*- and 4-positions, respectively. In this study, we synthesized and studied three mediators: 4-benzoyl-1-methylpyridinium chloride (BzM), 3-(4-benzoylpyridin-1-ium-1-yl)propane-1-sulfonate (BzSP), and 3-(4-acetylpyridin-1-ium-1-yl)propane-1-sulfonate (AcSP) (Fig. 1B). The proton-coupled redox behavior of the mediators and their  $\text{CO}_2$  capture/release mechanism is illustrated in Fig. 1C. During reduction, a pyridinium radical is formed, which takes up protons from the solution and enables  $\text{CO}_2$  capture. In the subsequent reoxidation stage, the pyridinium radical undergoes electron loss and deprotonation, triggering  $\text{CO}_2$  release. Overall, the mediators lower the energetic input required to generate a pH-swing, thus enabling energy-efficient  $\text{CO}_2$  capture.

## Results

### CVs of pyridinium redox mediators

Cyclic voltammetry (CV) in 1 M  $\text{KNO}_3$  (aq.) was used to screen the pH-swing mediators' electrochemical properties before capture/release tests. We started our exploration of this family of molecules with the previously reported BzM (Fig. 1B).<sup>19,20</sup> A conservative potential window was employed to limit the

mediators to one reduction, thus avoiding the known reversibility issues associated with further reduced acylpyridinium products (Fig. S8).<sup>19</sup> The redox process of BzM was first studied in solutions of varying pH to understand the influence of pH on reversibility and redox potential. The redox process is reversible at pH values above 11 but not at pH values below 10 (Fig. 2A), which implies a chemical step (protonation) when the concentration of  $\text{H}^+$  is sufficiently high (*i.e.* when  $\text{pH} < \text{p}K_a$ ). Moreover, CVs over a wide pH range show that the potential of BzM's first reduction is pH-dependent, with a change of approximately  $-49 \text{ mV pH}^{-1}$ , confirming a  $1 \text{ e}^-/1 \text{ H}^+$  proton-coupled electron transfer (Fig. 2B).<sup>21</sup> This is consistent with a previous study of BzM.<sup>20</sup> Taken together, these findings confirm that BzM can be electrochemically transformed into a base, which is the fundamental requirement of a pH-swing mediator.

A high mediator solubility in all redox stages is important to maximize the capture solution's  $\text{CO}_2$  capacity. BzM's solubility comes primarily from its positive charge, which disappears during the reduction step (unless protonated). Thus, to avoid possible solubility issues with BzM, we also synthesized BzSP, which bears a permanently anionic propylsulfonate group (Fig. 1B). These substituents have been used extensively as solubilizing groups for bispyridiniums (*i.e.* viologens) in aqueous redox-flow batteries.<sup>22–26</sup> Finally, AcSP was synthesized as a control mediator to evaluate the influence of the substituent at the 4-position (Fig. 1B). All mediators showed the expected signals in their NMR (Fig. S1–S6) and FTIR (Fig. S7) spectra. In unbuffered 1 M  $\text{KNO}_3$  (aq.), a clear redox event is

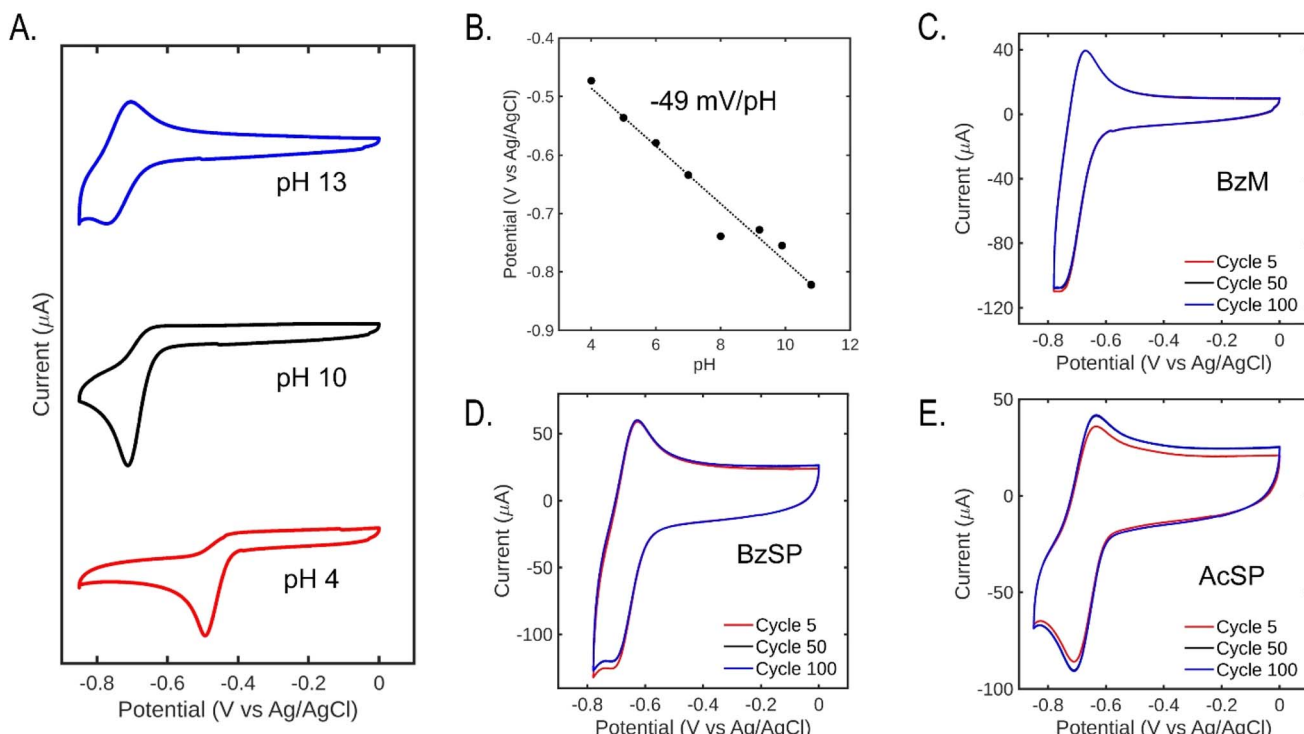


Fig. 2 Cyclic voltammetry of 5 mM pyridinium mediators at  $100 \text{ mV s}^{-1}$  under argon. (A) Cyclic voltammograms of BzM in various buffers with 1 M  $\text{KNO}_3$ . (B) Pourbaix diagram of BzM. (C–E) Long-term cyclic voltammograms in unbuffered 1 M  $\text{KNO}_3$  of BzM, BzSP, and AcSP.

observed at  $-0.71 \text{ V}$  vs.  $\text{Ag/AgCl}$  for BzM and  $-0.69 \text{ V}$  for BzSP and AcSP (Fig. 2C–E). The reduction of pyridinium mediators occurs within the pyridinium ring, and this structural feature is consistent in the three molecules, hence, the reduction potentials are similar. Prolonged CV experiments show slight variations in current in the early cycles, which is likely a result of local pH changes. However, the redox process quickly stabilizes and remains unchanged for at least 100 cycles. Finally, the reduction potentials of BzSP and AcSP also exhibit a strong pH-dependence, confirming the presence of PCET in these mediators (Fig. S9).

#### Carbon capture/release experiments in H-cell

Carbon capture/release experiments were carried out in an H-cell system (Fig. S10). The working electrode (WE) compartment contained 0.1 M pyridinium mediator and 1 M  $\text{KNO}_3$ , while the counter electrode (CE) compartment contained 0.1 M  $\text{K}_3\text{Fe}(\text{CN})_6$  and 0.2 M  $\text{K}_4\text{Fe}(\text{CN})_6$ , which served as an auxiliary redox couple. Pt coils were employed as WE and CE, with a  $\text{Ag}/\text{AgCl}$  (sat.  $\text{KCl}$ ) as the reference electron (RE), which was located in the WE compartment. A pH sensor and  $\text{CO}_2$  sensor provided real-time data on the capture/release process. Throughout the experiment, the solution in the WE compartment was continuously purged with a  $\text{CO}_2 : \text{N}_2$  mixture (10 : 90, v/v), which simulates an industrial flue gas stream. A  $\text{CO}_2$  concentration in the gas outlet lower than 10% corresponds to  $\text{CO}_2$  capture, while  $\text{CO}_2$  concentrations in the gas outlet higher than 10% indicate  $\text{CO}_2$  release. In the test of BzSP and AcSP, the WE and CE compartments were separated by a Nafion 117 cation

exchange membrane (CEM), which allows cation transport between the two compartments during the test. However, since BzM is a cation, prolonged experiments result in its migration across the CEM to the CE compartment. This crossover phenomenon causes progressive depletion of BzM in the working electrolyte, ultimately diminishing the  $\text{CO}_2$  capture capacity. Hence, in the test of BzM, a Fumasep FAA-3-PK-75 anion exchange membrane (AEM) was used to assemble the H-cell, and the electrolyte in the CE compartment comprised 0.2 M  $\text{FeCl}_2$  and 0.1 M  $\text{FeCl}_3$ .

Fig. S11 plots the CVs of three pyridinium mediators measured in the H-cell. The reduction current of BzM and BzSP is larger than AcSP, which follows the same trend as the CVs measured in diluted solution using the GC electrode, indicating that stabilizing benzoyl moiety facilitates electron transfer kinetics by increasing the stability of the reduction product. The reduction potential of BzSP ( $-0.78 \text{ V}$ ) is more positive compared to AcSP ( $-0.82 \text{ V}$ ) and BzM ( $-0.85 \text{ V}$  with Nafion membrane), which is also in the same trend as the results in a diluted solution.

Fig. 3A plots the results of the  $\text{CO}_2$  capture/release test using BzM as the redox mediator in the H-cell. During the experiment, the mediator was first reduced to generate a base, thus taking up protons from the solution and raising the pH. During this stage, acidic  $\text{CO}_2$  was captured by the solution and stored as (bi) carbonate ions. Based on the CV (red curve in Fig. S11A) measured in the H-cell, the reduction potential for BzM was set at  $-0.90 \text{ V}$  vs.  $\text{Ag/AgCl}$ . This potential was strategically set below the reduction potential of BzM, and above the hydrogen

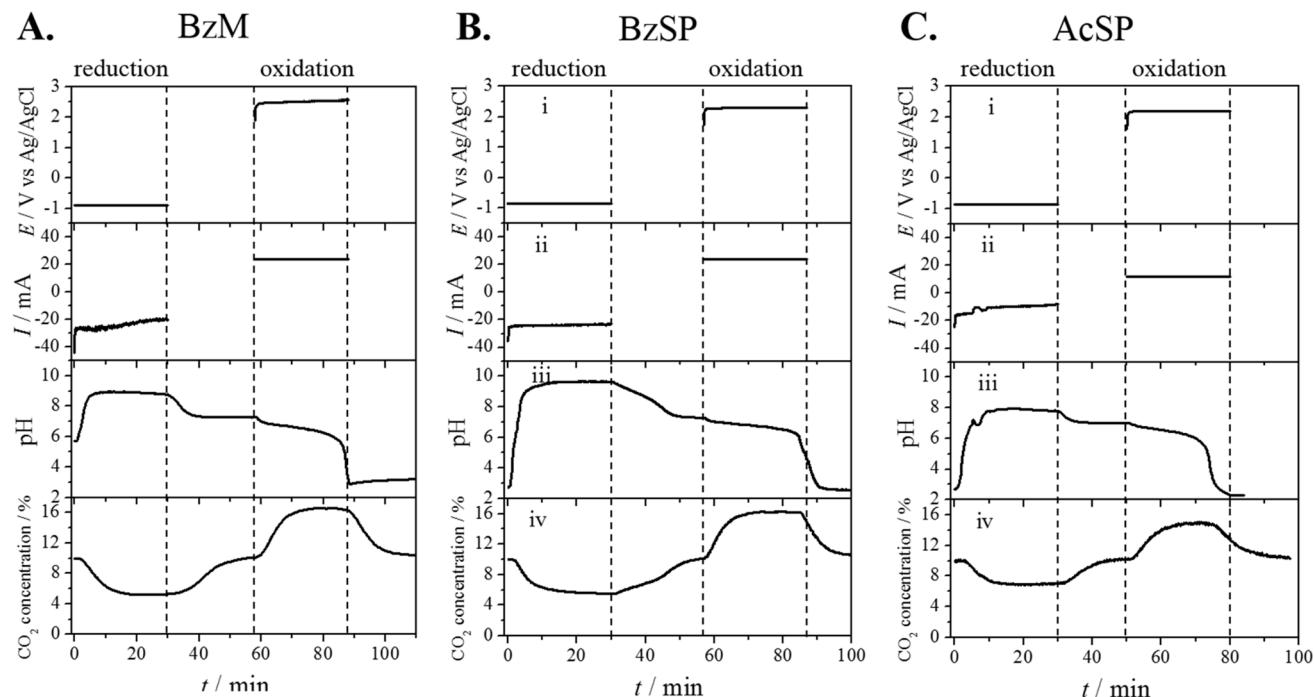


Fig. 3 H-cell  $\text{CO}_2$  capture/release tests. (A–C)  $\text{CO}_2$  capture/release results in the H-cell, (A) BzM, (B) BzSP, (C) AcSP. Fumasep AEM was used for BzM, and Nafion CEM was employed in the test of BzSP and AcSP. The pyridinium mediators were reduced using a constant potential and were reoxidized using a constant current. (i) Applied potential on the Pt WE, (ii) current of the Pt WE, (iii) pH of electrolyte in the WE compartment and (iv)  $\text{CO}_2$  concentration in the gas outlet.

evolution reaction (HER) potential on the Pt surface, thereby suppressing competitive  $\text{H}_2$  generation on the Pt coil. In Fig. 3A, the BzM reduction current was approximately  $-24.0\text{ mA}$ , accompanied by a gradual pH increase in the electrolyte. After 30 minutes of reduction, the potential was held at open circuit for 30 minutes to facilitate complete  $\text{CO}_2$  capture. The solution pH decreased to 7.3 during this additional invasion period.

BzM was subsequently reoxidized under constant-current conditions at  $24.0\text{ mA}$ , matching the average BzM reduction current. This condition ensured that the total charge passed through the Pt WE during the reduction and oxidation stages was balanced. The potential during BzM reoxidation was around  $+2.5\text{ V}$  vs.  $\text{Ag}/\text{AgCl}$ , demonstrating that the reoxidation process is energetically demanding and requires external energy input. Concurrent with reoxidation, the pH within the WE compartment underwent a pronounced decrease, falling from 7.3 to 2.9. This acidification of the electrolyte enabled the efficient release of captured  $\text{CO}_2$  from the solution. However, after the test, it was found that the  $\text{OH}^-$  anions generated in the reduction stage migrated across the AEM and formed  $\text{Fe}(\text{OH})_2$  and  $\text{Fe}(\text{OH})_3$  precipitates in the CE compartment. Hence, BzM is not a good candidate for the pH-swing  $\text{CO}_2$  capture/release.

Fig. 3B and C show the results of the  $\text{CO}_2$  capture/release test using BzSP and AcSP as the redox mediators. Based on the CVs (Fig. S11B & C) measured in the H-cell, the reduction potentials for BzSP and AcSP were set at  $-0.85$  and  $-0.90\text{ V}$  vs.  $\text{Ag}/\text{AgCl}$ , respectively. The average BzSP reduction current was  $-23.9\text{ mA}$ , higher than AcSP's  $-12.0\text{ mA}$ . Following 30 minutes of reduction, the potential was held at open circuit for 30 minutes

to ensure complete  $\text{CO}_2$  capture and proton regeneration. The mediators were then reoxidized in constant-current mode using currents equal to the absolute values of their respective reduction currents. BzSP demonstrates a better  $\text{CO}_2$  capture capacity compared to AcSP, as evidenced by three key metrics: (1) a larger current in the reduction stage, (2) a more alkaline post-reduction solution (pH 9.7 for BzSP vs. 7.9 for AcSP), and (3) greater  $\text{CO}_2$  concentration change in the gas outlet. These collective findings, as systematically demonstrated in Fig. 3B and C, establish BzSP's higher capacity in the pH-swing  $\text{CO}_2$  capture system. The amplified pH fluctuation and corresponding gas concentration changes directly correlate with its improved charge transfer efficiency.

To distinguish whether  $\text{CO}_2$  capture originates from the reduction of the pyridinium mediators or competing HER, a control experiment was performed in the H-cell containing exclusively  $1\text{ M KNO}_3$  in the WE compartment. Fig. S12A presents the carbon capture result obtained at a reduction potential of  $-0.85\text{ V}$ , which matches the potential applied for BzSP. The reduction current of  $1\text{ M KNO}_3$  without pyridinium mediator is between 1 and 2 mA, significantly lower than that observed in the electrolyte with  $0.1\text{ M BzSP}$ , indicating that HER is quite slow at this potential. Correspondingly, the change in pH and  $\text{CO}_2$  concentration is also small in the solution without the pyridinium mediator (Fig. S12B & C). The results in Fig. S12 indicate that the faradaic current in Fig. 3 predominantly arises from the reduction of the pyridinium mediators, with concomitant pH increase and  $\text{CO}_2$  capture being directly associated with this redox process rather than HER.



## Carbon capture/release experiments in a flow cell

From Fig. 3, it can be concluded that BzSP shows the best performance in the  $\text{CO}_2$  capture/release test. As the next step, we scaled up the synthesis of this champion mediator to a 20 g scale (see SI) and tested its energy efficiency for the  $\text{CO}_2$  capture/release in a more commercially relevant flow cell. The schematic diagram of the flow cell setup is displayed in Fig. 4A. The cell was assembled with a Nafion 117 membrane and  $4\text{ cm}^2$  carbon papers (Sigracet 22AA) as the working and counter electrodes. The negolyte contained 25 mL of 0.1 M pyridinium mediator in 1 M  $\text{KNO}_3$ , and the posolyte contained 40 mL of 0.1 M  $\text{K}_3\text{Fe}(\text{CN})_6$  and 0.2 M  $\text{K}_4\text{Fe}(\text{CN})_6$ . The negolyte was continuously purged with a  $\text{CO}_2 : \text{N}_2$  mixture (10 : 90, v/v), and the pH of the negolyte was monitored by a pH sensor. Two peristaltic pumps were used to circulate the negolyte and posolyte into the cell during the test.

Fig. 4B–E plots the results of pH-swing  $\text{CO}_2$  capture/release in the flow cell configuration. The redox cycling protocol applied reduction and oxidation current of  $\pm 20\text{ mA cm}^{-2}$ , respectively (Fig. 4C), with both stages maintained for 30 minutes to ensure equivalent total charge between the redox processes. In the first and second cycles, during the reduction stage, the cell potential was around  $-1.0\text{ V}$  (Fig. 4B), and the pH

of the negolyte rose from 3.6 to 8.5 (Fig. 4D) concomitant with  $\text{CO}_2$  concentration dropping from 10% to 2.9% (Fig. 4E), demonstrating  $\text{CO}_2$  capture through proton consumption. A subsequent equilibration period at OCP allowed for further  $\text{CO}_2$  uptake, as shown by a gradual decrease in pH to 7.2. In the reoxidation stage, the cell potential was between 1.4 and 1.6 V, triggering a decrease in pH to 2.3 and an increase in  $\text{CO}_2$  concentration to 25.2%, thereby confirming  $\text{CO}_2$  release through proton regeneration.<sup>13</sup>

In the  $\text{CO}_2$  concentration plot, the  $\text{CO}_2$  release peak is narrower than the capture peak, and the maximum  $\text{CO}_2$  concentration change in the oxidation stage is larger than that observed in the reduction stage. These results indicate that the rate of  $\text{CO}_2$  release is faster than the rate of  $\text{CO}_2$  capture. This difference arises because  $\text{CO}_2$  capture is controlled by  $\text{CO}_2$  absorption kinetics, while  $\text{CO}_2$  release is constrained by the applied current density.<sup>13</sup>

At the end of the second cycle, the reoxidation potential exhibits a sudden increase from 1.7 V to 1.9 V. This increase suggests that BzSP may be depleted within the electrolyte. Subsequently, during the third cycle, the reduction potential decreases to  $-1.6\text{ V}$  while the oxidation potential increases further to 1.9 V. The elevated cell potential indicates that water splitting, which requires higher energy than BzSP reduction, becomes the dominant reaction. The depletion of BzSP during cycling is further supported by post-mortem CV analysis from H-cell capture/release tests, where the redox peaks of BzSP greatly diminish after three cycles (Fig. S13). These results demonstrate that BzSP remains stable for approximately 16 hours, corresponding to two full cycles. The pH of the negolyte at the end of the third cycle is higher than that measured at the end of the first and second cycles. This increase results from BzSP degradation reactions, which consume  $\text{H}^+$  ions (see the next section for mechanistic studies of BzSP reduction).

The theoretical  $\text{CO}_2$  capture capacity of the BzSP solution can be calculated as:

$$C = nc_{\text{BzSP}}V \quad (1)$$

where  $n$ ,  $c_{\text{BzSP}}$ ,  $V$  are the number of electrons transferred per BzSP molecule during reduction/oxidation ( $n = 1$ ), concentration of BzSP, and volume of negolyte, respectively. Following 30 minutes of reduction at  $20\text{ mA cm}^{-2}$ , approximately 60% of the theoretical BzSP capacity was reduced. The amount of  $\text{CO}_2$  captured/released by BzSP can be calculated using the area of peaks in the  $\text{CO}_2$  concentration plot (Fig. 4E). The  $\text{CO}_2$  capture/release efficiency (CE) can be determined as the ratio between the moles of  $\text{CO}_2$  captured/released and moles of electrons transferred as:

$$\text{CE} = \frac{n_{\text{CO}_2}}{n_e} \times 100\% = \frac{vpFA_{\text{CO}_2}}{RTI} \times 100\% \quad (2)$$

where  $v$ ,  $p$ ,  $F$ ,  $A_{\text{CO}_2}$ ,  $R$ ,  $T$ ,  $I$ ,  $t$  are the flow rate of effluent gas, pressure, Faraday constant, area of the  $\text{CO}_2$  peak, ideal gas constant, temperature, current, and time, respectively. The energy efficiency (EE) of the flow cell can also be calculated as:

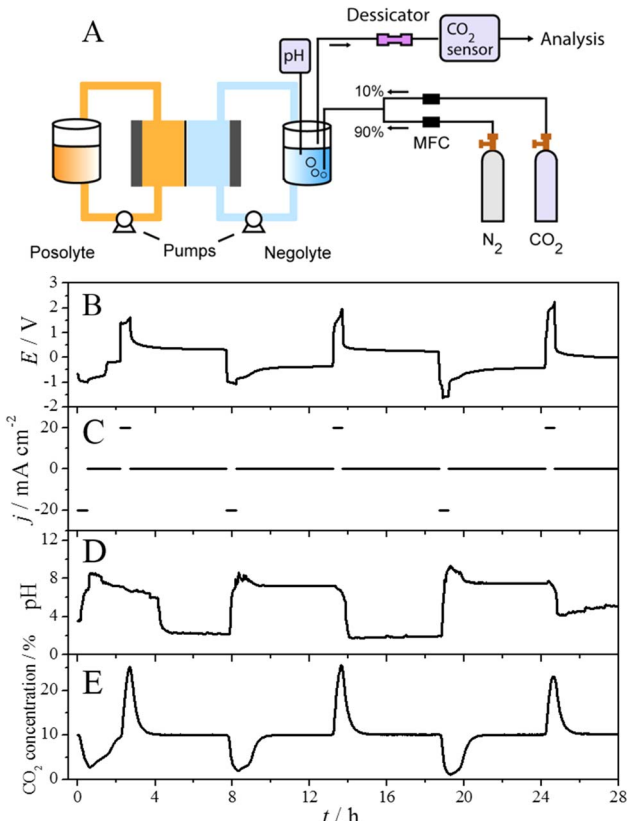


Fig. 4 (A) Schematic diagram of the flow cell system used in the pH-swing  $\text{CO}_2$  capture/release test. (B–E) Variation of the cell potential (B), current density of WE (C), pH of negolyte (D) and  $\text{CO}_2$  concentration (E) as a function of time during the  $\text{CO}_2$  capture/release test.



**Table 1**  $\text{CO}_2$  capture/release efficiency, energy efficiency and  $\text{CO}_2$  capture/release ratio using 0.1 M BzSP in the flow cell at a current density of 20 mA cm<sup>-2</sup>

	$\text{CO}_2$ capture/release efficiency/%	Energy efficiency/kJ mol $_{\text{CO}_2}$ <sup>-1</sup>	$\text{CO}_2$ capture/release ratio/%
Reduction cycle 1	90	102	88
Oxidation cycle 1	102	136	
Reduction cycle 2	89	108	84
Oxidation cycle 2	107	136	
Reduction cycle 3	94	143	98
Oxidation cycle 3	95	176	

$$\text{EE} = \frac{W}{n_{\text{CO}_2}} = \frac{EIt}{vpFA_{\text{CO}_2}/RT} \quad (3)$$

The  $\text{CO}_2$  capture/release ratio ( $C/R$ ) in one reduction–oxidation cycle is determined as:

$$C/R = \frac{A_{\text{CO}_2\text{-re}}}{A_{\text{CO}_2\text{-ox}}} \quad (4)$$

where  $A_{\text{CO}_2\text{-re}}$  and  $A_{\text{CO}_2\text{-ox}}$  are the area of the  $\text{CO}_2$  peak in the reduction and oxidation steps, respectively.

During the first two cycles, the  $\text{CO}_2$  capture/release efficiency is approximately 90% in the reduction stage and surpasses 100% in the oxidation stage (Table 1). The high efficiency in the oxidation stage may result from faster kinetics during  $\text{CO}_2$

release. In the third cycle, where water splitting occurs, the efficiency of the reduction and oxidation stages becomes similar. In the reduction stage of the first two cycles, the energy efficiency of  $\text{CO}_2$  capture is 102 kJ mol $_{\text{CO}_2}$ <sup>-1</sup>, and in the oxidation stage, the energy efficiency of  $\text{CO}_2$  release is 136 kJ mol $_{\text{CO}_2}$ <sup>-1</sup>. For the third cycle, the energy input increases for both stages due to the higher energy demand of water splitting compared to BzSP reduction and reoxidation.

The performance and energy efficiency of BzSP is compared with other reported redox mediators in Table S2. The reduction potential and  $\text{CO}_2$  capture energy efficiency of BzSP are competitive with state-of-the-art redox mediators.<sup>9,11,13,16</sup> However, a significant energy cost is incurred during the oxidation stage, resulting in an overall energy efficiency that is

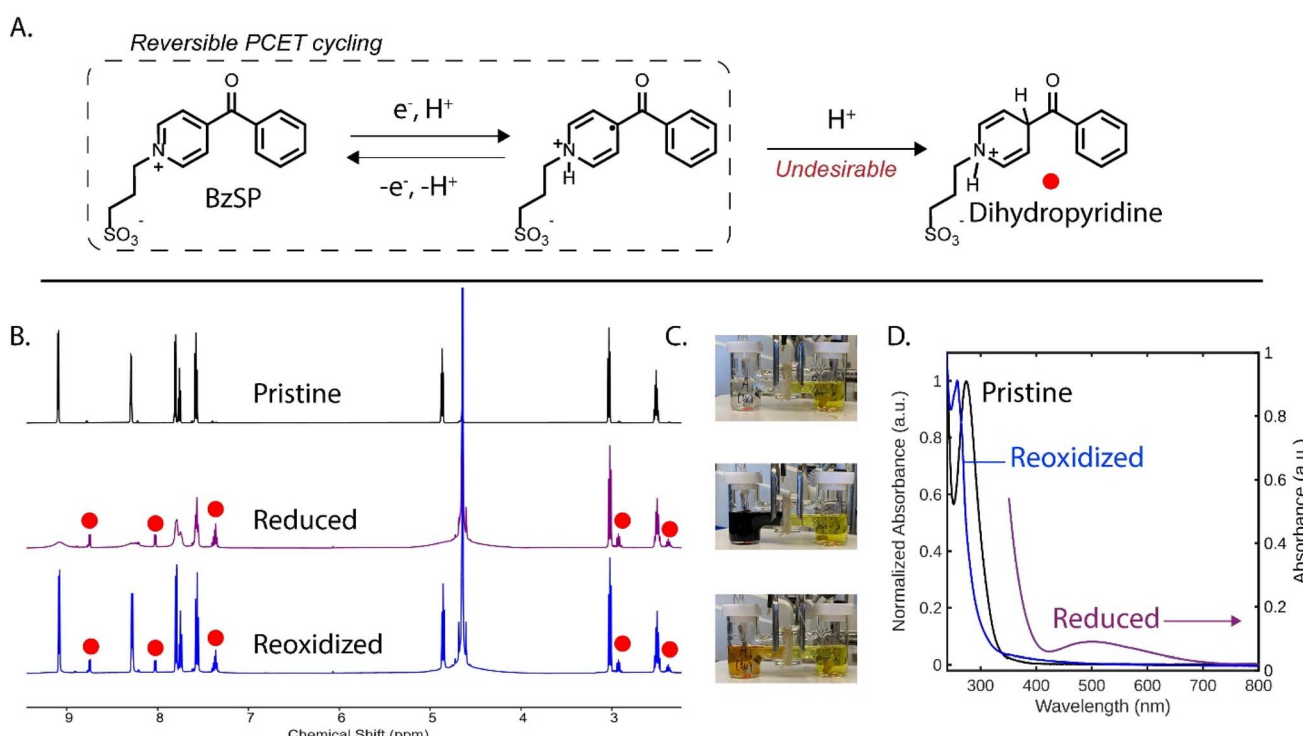


**Fig. 5** (A) Mechanism for BzSP-mediated  $\text{CO}_2$  capture, including degradation reaction to dihydropyridine. (B)  $^1\text{H}$  NMR spectra ( $\text{D}_2\text{O}$ , 500 MHz) of 0.1 M BzSP in 1 M  $\text{KNO}_3$  at different stages of the cycling process. (C) Photographs of the BzSP solution (left compartment) at each stage. (D) UV-visible absorption spectra at each stage. The pristine and reoxidized spectra are normalized, while the reduced spectrum is not. A large absorbance below 400 nm in the reduced spectrum is due to the high concentration of active species, which is necessary to observe the radical band.

currently higher than literature values for other mediators. To enhance the viability of our system, we are actively optimizing the oxidative process to improve its energy efficiency.

### Mechanistic studies

To gain insight into the mechanism of BzSP, we carried out a similar CO<sub>2</sub> capture/release experiment using D<sub>2</sub>O as the electrolyte solvent, thus enabling <sup>1</sup>H NMR analysis of the mediator at each stage of the process (Fig. 5B). Initially, the BzSP mediator is in its pristine state and its NMR peaks are aligned with those found in pure D<sub>2</sub>O. Following reduction, a broadening of the aromatic peaks is observed, consistent with the formation of radicals. This is further supported by UV-vis spectroscopy of the deep purple reduced capture solution (Fig. 5C), which shows a broad band centered at 500 nm (Fig. 5D).<sup>27</sup> Exposure of this solution to CO<sub>2</sub> leads to a new peak at 160 ppm in the <sup>13</sup>C NMR spectrum, which is attributed to HCO<sub>3</sub><sup>-</sup>, thus confirming successful sequestration of CO<sub>2</sub> (Fig. S14).

The NMR analysis is particularly useful for monitoring degradation. During reduction, small side peaks emerge in both the aromatic and aliphatic regions, indicating the formation of a new product with a very similar structure to BzSP (Fig. 5B). These peaks are still observed following oxidation and therefore represent a small loss of mediator over one capture/release cycle (approximately 11%). From mass spectrometry (Fig. S15) and further NMR studies (Fig. S16), the product is assigned as the dihydropyridine derivative of BzSP (Fig. 5A), which is consistent with previous work on pyridinium mediators.<sup>19</sup> Interestingly, the dihydropyridine signal does not increase following the oxidation step, implying that the degradation primarily occurs in the early stage of reduction, where some of the mediator is in radical form and pH is relatively low. Thus, improving the radicals' stability to H<sup>+</sup>-induced degradation is crucial to improving the cycle life of this CO<sub>2</sub> capture system. This has been achieved in organic solvents through careful design of the N- and 4-substituents.<sup>28</sup>

An experiment in D<sub>2</sub>O was also carried out for AcSP to understand its poor performance. Following reduction, the acetyl CH<sub>3</sub> signal is absent from the solution's <sup>1</sup>H NMR spectrum, indicating enolization and subsequent proton exchange with the solvent (Fig. S17), which is consistent with previous work.<sup>19</sup> The ability of AcSP to enolize means that it is susceptible to aldol reactions, and therefore has more available degradation pathways than BzSP.

## Conclusions

Three water-soluble pyridinium-based redox mediators (BzM, BzSP, AcSP) have been synthesized and evaluated for electrochemical pH-swing CO<sub>2</sub> capture/release, and we have identified structure–performance relationships, degradation mechanisms, and practical limitations. These molecules show reversible redox behavior and can electrochemically induce pH-swings, thus opening the door to CO<sub>2</sub> capture. In H-cell tests, BzSP demonstrates optimal CO<sub>2</sub> capture capacity, evidenced by

higher reduction currents, larger pH swings, and greater CO<sub>2</sub> concentration changes than AcSP and BzM. In a flow cell setup, BzSP exhibits stable operation for two full cycles (~16 h), achieving ~90% CO<sub>2</sub> capture efficiency and ~100% CO<sub>2</sub> release efficiency. The energy requirement for CO<sub>2</sub> capture is 102 kJ mol<sub>CO<sub>2</sub></sub><sup>-1</sup>, however, CO<sub>2</sub> release during oxidation requires significantly more energy (136 kJ mol<sub>CO<sub>2</sub></sub><sup>-1</sup>), highlighting a key area for optimization. Degradation of the molecules through an acid-induced pathway was observed, which limits the mediator lifetime. Future work will aim to lower the energetic input of the oxidation stage, to improve the cycling life through rational molecular engineering, and to carry out experiments with more practically relevant gas streams, which include oxygen and impurities such as SO<sub>x</sub> and NO<sub>x</sub>. Overall, this study establishes that the acylpyridinium family is suitable for electrochemically mediated CO<sub>2</sub> capture and paves the way for the development of new pH-swing redox mediators.

## Author contributions

EG, DS, PK, and SC conceived the project. EG and JTL carried out the synthesis. ZS carried out FTIR while EG and JTL carried out all other chemical characterization. EG, JTL, ZS, SC, and AL carried out electrochemical studies. AW helped with system design. ZS and SC carried out long-term CO<sub>2</sub> capture/release tests and analysis. EG and ZS drafted the manuscript and all authors contributed to revision. DS, PK, and SC supervised the project.

## Conflicts of interest

There are no conflicts to declare.

## Data availability

The authors confirm that the data supporting the findings of this study are available within the article and/or its SI. Supplementary information is available. See DOI: <https://doi.org/10.1039/d5sc04731e>.

## Acknowledgements

We gratefully acknowledge financial support provided by the Natural Sciences and Engineering Research Council of Canada (NSERC) Discovery Grants Program (RGPIN-2022-04319), the National Research Council (NRC) of Canada's Collaborative Centre for Green Energy Materials (CC-GEM), and the Materials for Clean Fuels (MCF) Challenge Program at the NRC. EG and JTL are grateful for graduate scholarships from NSERC.

## References

- 1 J. M. Barlow, L. E. Clarke, Z. Zhang, D. Bím, K. M. Ripley, A. Zito, F. R. Brushett, A. N. Alexandrova and J. Y. Yang, Molecular Design of Redox Carriers for Electrochemical CO<sub>2</sub> Capture and Concentration, *Chem. Soc. Rev.*, 2022, **51**(20), 8415–8433, DOI: [10.1039/D2CS00367H](https://doi.org/10.1039/D2CS00367H).



2 A. Ozden, CO<sub>2</sub> Capture *via* Electrochemical pH-Mediated Systems, *ACS Energy Lett.*, 2025, **10**, 1550–1576, DOI: [10.1021/acsenergylett.5c00200](https://doi.org/10.1021/acsenergylett.5c00200).

3 S. E. Renfrew, D. E. Starr and P. Strasser, Electrochemical Approaches toward CO<sub>2</sub> Capture and Concentration, *ACS Catal.*, 2020, **10**(21), 13058–13074, DOI: [10.1021/acscatal.0c03639](https://doi.org/10.1021/acscatal.0c03639).

4 M. Rahimi, A. Khurram, T. A. Hatton and B. Gallant, Electrochemical Carbon Capture Processes for Mitigation of CO<sub>2</sub> Emissions, *Chem. Soc. Rev.*, 2022, **51**(20), 8676–8695, DOI: [10.1039/D2CS00443G](https://doi.org/10.1039/D2CS00443G).

5 P. Singh, J. H. Rheinhardt, J. Z. Olson, P. Tarakeshwar, V. Mujica and D. A. Buttry, Electrochemical Capture and Release of Carbon Dioxide Using a Disulfide-Thiocarbonate Redox Cycle, *J. Am. Chem. Soc.*, 2017, **139**(3), 1033–1036, DOI: [10.1021/jacs.6b10806](https://doi.org/10.1021/jacs.6b10806).

6 R. Ranjan, J. Olson, P. Singh, E. D. Lorance, D. A. Buttry and I. R. Gould, Reversible Electrochemical Trapping of Carbon Dioxide Using 4,4'-Bipyridine That Does Not Require Thermal Activation, *J. Phys. Chem. Lett.*, 2015, **6**(24), 4943–4946, DOI: [10.1021/acs.jpclett.5b02220](https://doi.org/10.1021/acs.jpclett.5b02220).

7 S. Voskian and T. Alan Hatton, Faradaic Electro-Swing Reactive Adsorption for CO<sub>2</sub> Capture, *Energy Environ. Sci.*, 2019, **12**(12), 3530–3547, DOI: [10.1039/C9EE02412C](https://doi.org/10.1039/C9EE02412C).

8 H. Seo, M. P. Nitzsche and T. A. Hatton, Redox-Mediated pH Swing Systems for Electrochemical Carbon Capture, *Acc. Chem. Res.*, 2023, **56**(22), 3153–3164, DOI: [10.1021/acs.accounts.3c00430](https://doi.org/10.1021/acs.accounts.3c00430).

9 Y. Jing, K. Amini, D. Xi, S. Jin, A. M. Alfaraidi, E. F. Kerr, R. G. Gordon and M. J. Aziz, Electrochemically Induced CO<sub>2</sub> Capture Enabled by Aqueous Quinone Flow Chemistry, *ACS Energy Lett.*, 2024, **9**(7), 3526–3535, DOI: [10.1021/acsenergylett.4c01235](https://doi.org/10.1021/acsenergylett.4c01235).

10 C. Huang, C. Liu, K. Wu, H. Yue, S. Tang, H. Lu and B. Liang, CO<sub>2</sub> Capture from Flue Gas Using an Electrochemically Reversible Hydroquinone/Quinone Solution, *Energy Fuels*, 2019, **33**(4), 3380–3389, DOI: [10.1021/acs.energyfuels.8b04419](https://doi.org/10.1021/acs.energyfuels.8b04419).

11 S. Jin, M. Wu, R. G. Gordon, M. J. Aziz and D. G. Kwabi, pH Swing Cycle for CO<sub>2</sub> Capture Electrochemically Driven through Proton-Coupled Electron Transfer, *Energy Environ. Sci.*, 2020, **13**(10), 3706–3722, DOI: [10.1039/D0EE01834A](https://doi.org/10.1039/D0EE01834A).

12 H. Xie, Y. Wu, T. Liu, F. Wang, B. Chen and B. Liang, Low-Energy-Consumption Electrochemical CO<sub>2</sub> Capture Driven by Biomimetic Phenazine Derivatives Redox Medium, *Appl. Energy*, 2020, **259**, 114119, DOI: [10.1016/j.apenergy.2019.114119](https://doi.org/10.1016/j.apenergy.2019.114119).

13 S. Pang, S. Jin, F. Yang, M. Alberts, L. Li, D. Xi, R. G. Gordon, P. Wang, M. J. Aziz and Y. Ji, A Phenazine-Based High-Capacity and High-Stability Electrochemical CO<sub>2</sub> Capture Cell with Coupled Electricity Storage, *Nat. Energy*, 2023, **8**(10), 1126–1136, DOI: [10.1038/s41560-023-01347-z](https://doi.org/10.1038/s41560-023-01347-z).

14 H. Seo and T. A. Hatton, Electrochemical Direct Air Capture of CO<sub>2</sub> Using Neutral Red as Reversible Redox-Active Material, *Nat. Commun.*, 2023, **14**(1), 313, DOI: [10.1038/s41467-023-35866-w](https://doi.org/10.1038/s41467-023-35866-w).

15 S. Jin, M. Wu, Y. Jing, R. G. Gordon and M. J. Aziz, Low Energy Carbon Capture *via* Electrochemically Induced pH Swing with Electrochemical Rebalancing, *Nat. Commun.*, 2022, **13**(1), 1–11, DOI: [10.1038/s41467-022-29791-7](https://doi.org/10.1038/s41467-022-29791-7).

16 H. Seo, M. Rahimi and T. A. Hatton, Electrochemical Carbon Dioxide Capture and Release with a Redox-Active Amine, *J. Am. Chem. Soc.*, 2022, **144**(5), 2164–2170, DOI: [10.1021/jacs.1c10656](https://doi.org/10.1021/jacs.1c10656).

17 H. Xie, W. Jiang, T. Liu, Y. Wu, Y. Wang, B. Chen, D. Niu and B. Liang, Low-Energy Electrochemical Carbon Dioxide Capture Based on a Biological Redox Proton Carrier, *Cell Rep. Phys. Sci.*, 2020, **1**(5), 100046, DOI: [10.1016/j.xcrp.2020.100046](https://doi.org/10.1016/j.xcrp.2020.100046).

18 C. J. Li, J. W. Ziller, J. M. Barlow and J. Y. Yang, Aqueous Electrochemical and pH Studies of Redox-Active Guanidino Functionalized Aromatics for CO<sub>2</sub> Capture, *ACS Org. Inorg. Au*, 2024, **4**(4), 387–394, DOI: [10.1021/acs.orginorgau.3c00066](https://doi.org/10.1021/acs.orginorgau.3c00066).

19 C. S. Sevov, K. H. Hendriks and M. S. Sanford, Low-Potential Pyridinium Anolyte for Aqueous Redox Flow Batteries, *J. Phys. Chem. C*, 2017, **121**(44), 24376–24380, DOI: [10.1021/acs.jpcc.7b06247](https://doi.org/10.1021/acs.jpcc.7b06247).

20 A. Harriman, G. R. Millward, P. Neta, M. C. Richoux and J. M. Thomas, Interfacial Electron-Transfer Reactions between Platinum Colloids and Reducing Radicals in Aqueous Solution, *J. Phys. Chem.*, 1988, **92**(5), 1286–1290, DOI: [10.1021/j100316a054](https://doi.org/10.1021/j100316a054).

21 D. R. Weinberg, C. J. Gagliardi, J. F. Hull, C. F. Murphy, C. A. Kent, B. C. Westlake, A. Paul, D. H. Ess, D. G. McCafferty and T. J. Meyer, Proton-Coupled Electron Transfer, *Chem. Rev.*, 2012, **112**(7), 4016–4093, DOI: [10.1021/cr200177j](https://doi.org/10.1021/cr200177j).

22 C. DeBruler, B. Hu, J. Moss, J. Luo and T. L. Liu, A Sulfonate-Functionalized Viologen Enabling Neutral Cation Exchange, Aqueous Organic Redox Flow Batteries toward Renewable Energy Storage, *ACS Energy Lett.*, 2018, **3**(3), 663–668, DOI: [10.1021/acsenergylett.7b01302](https://doi.org/10.1021/acsenergylett.7b01302).

23 R. Rubio-Presa, L. Lubián, M. Borlaf, E. Ventosa and R. Sanz, Addressing Practical Use of Viologen-Derivatives in Redox Flow Batteries through Molecular Engineering, *ACS Mater. Lett.*, 2023, **5**(3), 798–802, DOI: [10.1021/acs.materialslett.2c01105](https://doi.org/10.1021/acs.materialslett.2c01105).

24 E. Grignon, J. T. Liu, Y. F. Tan, Y. Cao, A. Aspuru-Guzik and D. S. Seferos, Highly Water-Soluble Polyether-Based Viologen Negolytes for Aqueous Redox-Flow Batteries, *J. Am. Chem. Soc.*, 2025, **147**(6), 5071–5079, DOI: [10.1021/jacs.4c14969](https://doi.org/10.1021/jacs.4c14969).

25 A. Debiais, C. Lai, T. Boulanger, G. Reynard, L. Hamlet, S. Généreux, M. Vaillancourt, R. Iftimie, H. Lebel and D. Rochefort, Highly Soluble Viologen-PEG Conjugates for Aqueous Organic Redox Flow Batteries, *ACS Appl. Energy Mater.*, 2025, **8**(1), 181–193, DOI: [10.1021/acsaelm.4c02259](https://doi.org/10.1021/acsaelm.4c02259).

26 P. T. Sullivan, H. Liu, X.-L. Lv, S. Jin, W. Li and D. Feng,

Viologen Hydrothermal Synthesis and Structure–Property Relationships for Redox Flow Battery Optimization, *Adv. Energy Mater.*, 2023, 13(34), 2203919, DOI: [10.1002/aenm.202203919](https://doi.org/10.1002/aenm.202203919).

27 E. M. Kosower, Stable Pyridinyl Radicals, in *Preparative Organic Chemistry*, Springer, Berlin, 1983, pp. 117–162, DOI: [10.1007/3-540-12396-2\\_7](https://doi.org/10.1007/3-540-12396-2_7).

28 C. S. Sevov, D. P. Hickey, M. E. Cook, S. G. Robinson, S. Barnett, S. D. Minteer, M. S. Sigman and M. S. Sanford, Physical Organic Approach to Persistent, Cyclable, Low-Potential Electrolytes for Flow Battery Applications, *J. Am. Chem. Soc.*, 2017, 139(8), 2924–2927, DOI: [10.1021/jacs.7b00147](https://doi.org/10.1021/jacs.7b00147).